Interaction of Escherichia coli heat-labile enterotoxin B-pentamer with exopolysaccharides from Leuconostoc mesenteroides P35: Insights from surface plasmon resonance and molecular docking studies

Mojtaba Azari-Anpar, Pascal Degraeve, Nadia Oulahal, Isabelle Adt, Kambiz Jahanbin, Yann Demarigny, Ali Assifaoui, Farideh Tabatabaei Yazdi

Author contributions

Mojtaba AZARI-ANPAR: conceptualization, investigation, writing - original draft ; Pascal DEGRAEVE: conceptualization, resources, supervision, methodology, writing: review & editing ; Nadia OULAHAL: conceptualization, supervision, methodology, writing - review & editing ; Isabelle ADT: investigation (FTIR spectroscopy experiments, exopolysaccharides purification and characterization), writing - review & editing; Kambiz JAHANBIN: investigation (surface plasmon resonance experiments), methodology, writing - review & editing; Yann DEMARIGNY: investigation (exopolysaccharides production) ; Ali ASSIFAOUI, investigation (zeta potential measurement and interpretation), Farideh TABATABAEI YAZDI : conceptualization, resources, supervision, methodology, writing: review & editing.

Highlights

- *E. coli* heat-labile enterotoxin B-pentamer was immobilized on a surface sensor.
- *Ln. mesenteroides* P35 exopolysaccharides had a high affinity for *E. coli* enterotoxin.
- Thermodynamic analysis of binding suggests a dominant contribution of hydrophobic forces.
- Molecular docking suggests putative binding sites along *E. coli* enterotoxin sequence.

Interaction of *Escherichia coli* heat-labile enterotoxin B-pentamer with exopolysaccharides from *Leuconostoc mesenteroides* P35: Insights from surface plasmon resonance and molecular docking studies

Mojtaba Azari-Anpar[a,b], Pascal Degraeve[a], Nadia Oulahal[a], Isabelle Adt[a], Kambiz Jahanbin[c], Yann Demarigny[a], Ali Assifaoui[d], Farideh Tabatabaei Yazdi[b *]

[a] Univ Lyon, Université Claude Bernard Lyon 1, ISARA Lyon, BioDyMIA Research Unit, 155 rue Henri de Boissieu, F-01000, Bourg en Bresse, France

[b] Ferdowsi University of Mashhad, Faculty of Agriculture, Department of Food Science and Technology, Mashhad 91775-1163, Iran

[c] Shahrood University of Technology, Faculty of Agricultural Engineering, Department of Food Science and Technology, P.O. Box 361999-5161, Shahrood, Iran

[d] Unité Mixte de Recherche Procédés Alimentaires et Microbiologiques, Université de Bourgogne Franche-Comté (UBFC), UMR PAM A 02.102, 21000 Dijon, France

E-mail address of each author

Mojtaba AZARI-ANPAR, Email address: mojtaba.azari-anpar@etu.univ-lyon1.fr

Pascal DEGRAEVE, Email address: pascal.degraeve@univ-lyon1.fr

Nadia OULAHAL, Email address: nadia.oulahal@univ-lyon1.fr

Isabelle ADT, Email address: isabelle.adt@univ-lyon1.fr

Kambiz JAHANBIN, Email address: Jahanbin@shahroodut.ac.ir

Yann DEMARIGNY, Email address: ydemarigny@isara.fr

Ali ASSIFAOUI, Email address: ali.assifaoui@u-bourgogne.fr

Farideh TABATABAEI YAZDI, Email address: tabatabai@um.ac.ir

*Corresponding author's email: tabatabai@um.ac.ir

*Corresponding author's phone number: 00989155138415

Abstract

In this study, the interaction of exopolysaccharides from *Leuconostoc mesenteroides* P35 (EPS-LM) with *Escherichia coli* heat-labile enterotoxin B-pentamer (LTB) was investigated at different concentrations and temperatures by using surface plasmon resonance (SPR) and molecular docking approaches. FT-IR spectral analysis together with HPTLC analysis revealing that glucose is the only constitutive monosaccharide of EPS-LM suggests that its structure is composed of dextran with α-D (1→6) glycosidic linkages. SPR analysis revealed the high affinity of EPS-LM for immobilized LTB toxin (K_A=(2.05 ± 0.04) ×10^6 mol.L^{-1} at 37°C). The binding process was spontaneous (ΔG<0), endothermic (ΔH>0), and entropy-driven (ΔS>0) with an increase of K_A with temperature. This suggests that EPS-LM - LTB interaction is dominated by hydrophobic forces. The binding affinity of EPS-LM to LTB had negligible dependence on enthalpy (ΔH= 0.084 kJ.mol^{-1}). Further, molecular docking results suggested the presence of some binding sites of EPS-LM on the LTB through hydrophobic forces (Lys, Asp, Arg, Glu) and also hydrogen bonding (Glu) in the hydrophobic core of LTB. Besides autodock studies, Schiffer-Edmundson helical wheel diagrams of LTB in α-helix domain suggested that LTB hydrophobic core is a highly effective region, which was able to form favorable non-polar interactions of the protein's binding surface (with amino acids residues such as Tyr, Leu, Ile) with EPS-LM. This study provided thus further insights into the interactions between EPS-LM and LTB, suggesting that EPS produced by some LAB, such as EPS produced by *Ln. mesenteroides* P35 strain are good candidates to inhibit *E. coli* toxin activity.

Keywords: *Escherichia coli* heat-labile enterotoxin, exopolysaccharide, interaction, surface plasmon resonance, detoxification.

1. Introduction

Enterotoxigenic *Escherichia coli* (ETEC) has been estimated to account for approximately 210 million diarrhea episodes annually, being thus the most frequently isolated enteropathogen. This diarrhea is initiated by the binding of B subunit of heat-labile enterotoxin (LTB) to the ganglioside GM_1 on the

surface of intestinal epithelial cells. Therefore, different authors have investigated the possibility to inhibit LTB interaction with GM_1. For instance, Chen et al. (2006) screened the inhibitory effects of 297 Chinese medicinal herbs on the LTB and GM1 interaction. Interestingly, *Galla Chinensis* extract and its main component, gallic acid, inhibited the binding of LTB with GM1. Moreover, these authors speculated that gallic acid might interact with LTB through similar hydrogen bonds than those involved in its interaction with terminal galactose of exposed oligosaccharide head group of GM1. Indeed, hydrogen bonds with this part of GM1 have been suggested to be important for the binding of LTB (Pickens et al., 2002). The same group used *in silico* analysis (molecular docking) to predict the phytochemicals of traditional medicinal plants, which are likely to interact with LTB (Chen et al., 2009). This allowed them to identify triterpenoids, especially oleanane type, as compounds with a high affinity for LTB. This was confirmed by *in vitro* analysis, and *in vivo* analysis following patent mouse gut (non-occluded gut) assay confirmed their capacity to inhibit LT-induced diarrhea.

In the present study, the interaction of exopolysaccharides (EPS) produced by lactic acid bacteria with LTB was investigated. Since LTB interacts with terminal galactose of exposed head group of GM1, it is likely that some EPS can interact with the same zone of LTB, thereby inhibiting its interaction with GM1 if the affinity of EPS for LTB is sufficient. Many *Leuconostoc mesenteroides* strains produce high amounts of EPS, such as dextran and are commonly used as a starter in many fermented foods (e. g. dairy products, sourdough…). Therefore, EPS produced in a whey-based medium, with a *Ln. mesenteroides* strain selected for its capacity to produce high amounts of EPS, *Ln. mesenteroides* P35 (Gemelas et al., 2018) were purified, partially characterized, and subsequently used to investigate their interaction with LTB toxin. While there is an increasing interest for health-promoting properties of lactic acid bacteria EPS (as recently reviewed by Jurášková et al. (2022)) and while probiotic lactic acid bacteria have been proposed to be promising biological detoxification tools of food chemical contamination by different ways including the production of metabolites acting by adsorption of toxins (Srednicka et al., 2021), to our knowledge, this is the first investigation of LTB toxin-EPS interactions. In the present study, interactions between *Ln. mesenteroides* P35 EPS and LTB toxin were first investigated by surface plasmon resonance following immobilization of LTB toxin by amine coupling on an amine carboxymethyl dextran sensor chip. *In silico* analysis by molecular docking of interactions

between LTB toxin and *Ln. mesenteroides* P35 EPS allowed then to precise the putative corresponding molecular interactions involved.

2. Materials and methods

2.1. Microorganism and growth conditions

Ln. mesenteroides strain P35 was isolated from microbiota of raw milk goat cheese (Ardèche, France) by ISARA (Lyon, France). EPS production was performed by cultivating this strain under conditions determined by Gemelas et al. (2018) to favour the production of these extracellular metabolites. Briefly, a pre-fermentation step consisted in culturing aerobically for 16 h at 25°C with vigorously shaking *Ln. mesenteroides* P35 in a reconstituted whey solution (10% (w/v) whey powder, Eurosérum, St Martin Belle Roche, France) and sucrose 2% into Erlenmeyer flasks and sterilized at 110°C for 10 min. Then, this whey-based medium was supplemented with sucrose (5% w/v) and cultured under constant shaking at 100 rpm at 20 °C. The production of EPS was followed daily by measuring the increase of viscosity.

2.2. Extraction and purification of EPS-LM

To extract *Ln. mesenteroides* strain P35 EPS (EPS-LM), the fermented medium was diluted by adding Milli-Q water (50:50 v/v). The diluted suspension was stirred gently at 95 °C for 15 min to inactivate enzymes. This suspension was then cooled at room temperature and centrifuged (10000 ×g for 20 min). For depleting protein, the supernatant was treated twice with Sevag reagent (chloroform: n-butanol, 5:1 v/v). By adding pre-chilled ethanol (-20 °C; 96% (v:v)) to supernatant (three volumes ethanol for 1 volume of supernatant), EPS were precipitated. The obtained EPS pellet was then resuspended in Milli Q water and dialyzed by using a cellulose dialysis bag (MWCO (molecular weight cut-off): 12-14 kDa, Spectra/Por®, Spectrum Chemical Mfg. Corp., New Brunswick, NJ, USA) against Milli-Q water for 48 h at 4 °C and then freeze-dried and stored at -18°C (Saravanan and Shetty, 2016).

The crude EPS-LM were purified by methods described by Zhang et al. (2017) with slight modifications. The EPS-LM were resuspended in sodium acetate buffer (pH 5.5; 10 mM) at a concentration of 1.5 $g.L^{-1}$ and purified using anion-exchange chromatography with a HiPrep™ Q HP 16/10 column (GE Healthcare Bio-Sciences AB Björkgatan, Uppsala Sweden). The system was adjusted on UV variable wavelengths (215, 220, 280 nm) in order to detect peptides, DNA, and proteins, respectively. EPS were eluted with the same buffer at a flow rate of 3 mL/min followed by a linear NaCl gradient ranging from

0 to 2 M in sodium acetate buffer at a flow rate of 3 mL/min. The process was carried out on a FPLC system (Äkta pure 25, Uppsala, Sweden). Each eluted fraction (5 mL) was collected, and at the end of chromatographic separation, the EPS content of each fraction was assayed using the phenol-sulfuric acid method. Protein content of each fraction was assayed with a Micro BCA protein assay Kit (Thermo Fisher Scientific, Illkirch-Graffenstaden, France). Finally, major EPS-containing fractions were combined. After dialysis (MWCO: 12-14 kDa) against Milli-Q water, the EPS were dried and used as the purified EPS-LM (Zhang et al., 2017).

2.3. Constitutive monosaccharides analysis using HPTLC (High Performance Thin Layer Chromatography)

The composition of EPS-LM was investigated using the method of Saravanan and Shetty (2016) with a slight modification. In brief, 3 mg from the EPS-LM and following monosaccharides standards (glucose, galactose, mannose, rhamnose, fructose, glucuronic acid, galacturonic acid, xylose, arabinose) and 1 mL trifluoroacetic acid (TFA (2M)) were mixed and hydrolyzed at 121 °C for 4 h in an oven. Separation and identification of the hydrolysates (5 µL) were uniformly carried out by HPTLC plate (TLC Silica gel 60 F_{254} with a 20 × 2.5 cm concentrating zone, Merck, Darmstadt, Germany) using a Camag® Linomat 5 HPTLC system (Muttenz, Switzerland). The chamber was prepared with enough solvent to cover the bottom of HPTLC plate. The solvent was composed of 10 mL distilled water, 30 mL ethyl acetate, and 20 mL acetic acid to saturate the atmosphere with solvent vapors for 1 h before putting the HPTLC plate in the chamber. Then the HPTLC plate was immersed in the developing solution until the solvent front reaches the top of the plate. Afterward, the HPTLC plate was visualized with injection of 2 mL TLC visualization reagent, in which 1g diphenylamine and 1mL aniline were dissolved first with 40 mL of methanol and then 5 mL of phosphoric acid (85%) was added before adjusting the final volume to 50 mL with methanol, with a Camag derivatizer and then heated at 100 °C for 30 min to visualize the bands. Finally, the retention factor (R_f) value was calculated for each monosaccharide according to Eq. 1 (Saravanan and Shetty, 2016):

$$R_f \text{ value} = \frac{Distance\ migrated\ by\ the\ monosaccharide}{Distance\ migrated\ by\ the\ solvent\ front} \quad \text{(Eq. 1)}$$

2.4. Fourier-transform infrared (FTIR) spectral analysis of EPS

The FTIR spectrum of the purified EPS-LM was collected in a transmission mode using macro compartment of IS50 system (Thermo Fischer, Illkirch-Graffenstaden, France). The major functional groups of the EPS-LM were determined by pressing the EPS sample into KBr pellets prepared by mixing EPS with KBr with a 1:100 (w:w) EPS: KBr ratio. The FTIR spectrum was recorded in the region of 4000-400 cm^{-1} wavenumbers with 32 scans with an infrared spectral resolution of 4 cm^{-1} (Nambiar et al., 2018).

2.5. Zeta potential (*Zp*) measurement of EPS-LM and net charge prediction and structural analysis of LTB toxin

Zp of EPS-LM (1 $g.L^{-1}$ in Milli-Q water) as a function of pH was determined with a ZetaCompact zetameter (CAD Instruments, Illiers-Combray, France). Sodium phosphate buffers (10 mM) with pHs of 2, 3, 4, 5, 6 and 7 were used to measure *Zp* at room temperature (~ 23 °C) and at the same ionic strength (10 mM). Briefly, the EPS-LM dispersion was placed manually with a syringe into a glass capillary, and the migration to the anode was monitored by optical microscopy with the zetameter. In fact, the ZetaCompact zetameter is based on micro-electrophoresis, which combines direct observation (microscopy) with particle mobility in an electric field (electrophoresis). Particles motion was recorded with a high-sensitivity digital camera (Ayala-Torres et al., 2014). As well, the Helmholtz-Smoluchowski model was used to calculate the zeta potential from particle electrophoretic mobility (Hiemenz and Rajagopalan.,1977). PepCalc.com-Peptide property calculator web server (Innovagen AB, https://pepcalc.com) was used to compute the net charge(Jiménez-Vargas et al., 2021). Amino acid sequence to predict the structural properties of LTB toxin (Sigma-Aldrich, E8656) according to previous literature (PDB ID: 1EFI) was used. The amino acid one-letter code primary sequence for modeling and estimation of its structure was as follows:

APQTITELCSEYRNTQIYTINDKILSYTESMAGKREMVIITFKSGETFQVEVPGSQHIDSQKKAI ERMKDTLRITYLTETKIDKLCVWNNKTPNSIAAISMKN.

2.6. Surface Plasmon Resonance (SPR) analysis of *Escherichia coli* heat-labile enterotoxin B-pentamer - exopolysaccharides from *Leuconostoc mesenteroides* P35 interactions

The kinetic and thermodynamic parameters were determined by using a SPR sensing device with two different dual-channel detections, which utilizes a prism based on the Kretscheman configuration (MP-

SPR Navi 210A, BioNavis Ltd, Tampere-region, Finland). The analyte concentrations were confirmed before the final SPR experiment and before the SPR assay, the whole flow path was rinsed with sodium phosphate buffer (10 mM; pH = 5.5) as running buffer. The interaction analysis was performed at a fixed angle at 670 nm wavelength and 25°C (Dehghani et al., 2021).

2.6.1. Formation of 11-mercaptoundecanoic acid (MUA) self-assembled monolayer (SAM) and LTB toxin immobilization

In this study, 11-mercaptoundecanoic acid (MUA) functionalized Au-coated SPR chips were used as SPR biosensor chips (Bionavis, Finland) (Figure. 1). In brief, 11-MUA chips were synthesized by immersion of Au-coated sensor chips in a hot solution containing 30% ammonia, 30% hydrogen peroxide (H_2O_2), and Milli-Q water (1:1:5, v/v/v) at 90 °C for 15 min. Then, chips were washed with Milli Q water and absolute ethanol, and dried under a N_2 gas stream. Afterward, they were obtained by treatment of 5 mM 11-MUA solution in ethanol and Milli-Q water (7:3, v/v) for 24 h at 25 °C and gently washed by either a triple rinsing with Milli-Q water and with sodium phosphate buffer (10 mM; pH = 5.5) and dried under N_2 gas.

To immobilize the LTB toxin on 11-MUA modified chips, N-ethyl- N-(3-diethyl aminopropyl) carbodiimide (EDC) / N-hydroxysuccinimide (NHS) were applied to form amine-based immobilization using an amine-to-amine crosslinker (via covalent amide binding). However, the 11-MUA-modified chips were inserted in the SPR device and rinsed with sodium phosphate buffer to attain a steady baseline in the sensorgram. Furthermore, the surface of the embedded chips was washed by injecting NaOH (0.01 M) and NaCl (2 M) in both channels for 2 min with a 30 µL/min flow rate at 25 °C. LTB toxin was then immobilized via covalent amide binding on a carboxymethyl dextran (CMD) hydrogel sensor chip through EDC/NHS 1:1 (NHS 0.05 M + EDC 0.2 M) solution in 10 mM sodium phosphate buffer (pH = 5.5) for 5 min with a 30 µL/min flow rate at 25 °C. Then, LTB toxin immobilization was accomplished by injecting LTB toxin solution (0.25 mg/mL) to channel 1 for 8 min and injection of phosphate buffer (running buffer) to channel 2 (reference channel). Finally, to prevent non-specific binding of detection ligands (LTB toxin) during the steps following transfer, unoccupied sites on the chip's surface were blocked through capping residual NHS esters with 1 M ethanolamine for 5 min so that no more compounds can be immobilized to the surface matrix during analyte injection (Fathi et al., 2019).

Fig 1.

2.6.2. Kinetic parameters of LTB toxin interaction with *Ln. mesenteroides* P35 EPS

The interactions between *Ln. mesenteroides* P35 EPS (0.25, 0.50, 1 and 2.0 mg. mL^{-1} in 10 mM sodium phosphate buffer, pH=7) and immobilized LTB toxin were investigated by SPR at pH 7 and different temperatures (298, 303, 310 K). To avoid the mass transfer effect, the SPR tests were carried out at a high flow rate (30 $\mu l.min^{-1}$) (Dehghani et al., 2021; Diemer, et al., 2012). Two flow cells for sample injection have been used: the channel without any LTB toxin and the channel with immobilized LTB toxin were the measurement channel and the reference channel, respectively. The rapid dissociation of EPS-LM from LTB toxin surface eliminated the necessity of the regeneration process. To evaluate the kinetic parameters upon the interaction of LTB toxin with EPS-LM, calculation of the association (k_a) and dissociation (k_d) rate constants and the equilibrium constants (K_A) is required. In general, ligand affinity to various biomacromolecules receptors such as LTB toxin can be defined as $K_A=k_a/k_d$ (Dehghani et al., 2021). To calculate kinetic parameters, Trace Drawer™ for SPR Navi™ was used through fitting Langmuir model (Oshannessy, et al., 1993), which describes a stoichiometry of 1:1. The Trace Drawer data were extracted with SPR Navi™ Data viewer software prior to any calculations.

2.6.3. Thermodynamic analysis

To assess the impact of temperature on LTB toxin and EPS-LM interactions, the thermodynamic parameters of LTB toxin/EPS-LM complex formation were systematically investigated. Therefore, SPR experiments have been performed at three different temperatures (298, 303, 310 K). Thermodynamic parameters (enthalpy change (ΔH°) and entropy change (ΔS°)) for LTB toxin/EPS-LM complex formation have been calculated by substituting K_A with $1/K_D$ into the van't Hoff equation and through plotting of ln K_A versus 1/T using Van't Hoff equation (Eq. 2). The Van't Hoff equation relates to the change in the equilibrium constant (Dehghani et al., 2021).

$$Ln\ K_A = -\frac{\Delta H^\circ}{RT} + \frac{\Delta S^\circ}{R} \qquad \text{(Eq. 2)}$$

where R represents the gas constant, T is absolute temperature, and ΔH° and ΔS° refer to standard enthalpy and entropy changes, respectively. After acquiring the ΔH° and ΔS° values, the ΔG° values were calculated using the Gibbs free energy equation (Eq. 3).

$$\Delta G^\circ = \Delta H^\circ - T\Delta S^\circ \quad \text{(Eq. 3)}$$

2.7. Molecular modelling and investigation of involved regions

LTB toxin protein and its amino acids sequence (PDB ID: 1EFI) have been downloaded from protein data bank website (https://www.rcsb.org/) and EPS-LM as our ligand exploited from Glycam-Web (https://dev.glycam.org/) and Sweet II (http://www.glycosciences.de/). In brief, structures of EPS-LM were generated in Glycam-Web by creating the Program Database File (.PDB) format, and then conformations of monosaccharides of EPS-LM were confirmed by rechecking from the Sweet II and PubChem Compound Database. All PDB formats were converted to PDBQT. Afterward, grid box center coordinates for LTB with EPS-LM were placed at x: -0.442, y: -3.836, and z: 17.328 Å to determine the total interaction energy between LTB and EPS-LM. The lowest free energy (ΔG) of docked complexes was determined after runs of docking. Finally, AutoDock Vina and LigPlot$^+$ version v.1.4.5 were used for estimating the interactions and binding energies of the obtained docked structures (Dehghani et al., 2021). The HeliQuest web server (http://heliquest.ipmc.cnrs.fr) was also used to calculate LTB toxin physico-chemical parameters, such as hydrophobicity and hydrophobic moment (Jiménez-Vargas, et al., 2021).

3. Results and discussion

3.1. Partial characterization of *Leuconostoc mesenteroides* P35 exopolysaccharides

3.1.1. Identification of constitutive monosaccharides of *Leuconostoc mesenteroides* P35 exopolysaccharides

Figure 2 shows the HPTLC plate spotted with hydrolyzed EPS-LM and standard solutions of different monosaccharides. The used method was able to separate the spots well, and the color development occurred after the derivatization step. The derivatization reagent facilitated the visualization of each monosaccharide. As a result of HPTLC analysis, the unique monosaccharides band of hydrolyzed EPS-LM shows one closely spaced spot with a R_f of 0.53. According to R_f close to that of glucose and

previous researchers that reported a R_f of 0.54 for glucose (Saravanan and Shetty, 2016), the unique monosaccharide band of hydrolyzed EPS-LM can be ascribed to glucose. Glucose was thus the only identified monosaccharide in the EPS-LM hydrolysate. This indicates that EPS-LM is a homopolysaccharide that is composed of repeating glucose units and is thus a glucan (Saravanan and Shetty, 2016).

Fig. 2.

3.1.2. FT-IR spectral analysis of *Leuconostoc mesenteroides* P35 exopolysaccharides

The FT-IR spectrum of the EPS-LM indicated the presence of a significant number of hydroxyl groups (O-H) in their structures, as it displayed a broad and intense stretching peak around 3419 cm^{-1}, thereby confirming the polysaccharide nature of the material (Purama et al., 2009; Siddiqui et al., 2014) (Figure 3). The bands present at 2924.6 cm^{-1} can be attributed to the C-H stretching vibration in CH_2 of C_6 position of the ring forms of glucose subunits of EPS-LM, as reported by several authors having analyzed by FTIR spectroscopy dextran produced by other *Ln. mesenteroides* strains (Purama et al., 2009; Siddiqui et al., 2014). The band at 1645 cm^{-1} was likely caused by the -OH bending vibration of water, while absorption peaks at 1459 and 1384 cm^{-1} were assigned to the vibration of C–H bond (Benvidi and Jahanbin, 2020). The wavenumbers ranging from 900 to 1200 cm^{-1} are known as fingerprints of carbohydrate structures due to glycosidic bonds. Absorbances with a wavenumber around 1015 cm^{-1} likely result from C-O in alcoholic groups (C-O-H). In general, the presence of these absorbances along with absorbances related to O-H groups (around 3400 cm^{-1}) confirmed the existence of carbohydrate structures. Peak levels, or rates of absorbances in both mentioned values (O-H groups and C-O bonds) can be considered as fingerprints of EPS. Since glycosidic bonds (C-O-C) are one type of ether bond (C-O), absorbance observed around 1158 cm^{-1} in EPS-LM confirmed the existence of ether bands (Shingel et al., 2002; Purama et al., 2009; Siddiqui et al., 2014). Absorbances below 1000 cm^{-1} of FT-IR spectra are consistent with the existence of pyranose (around 770 cm^{-1}) and furanose units (around 800 cm^{-1}) and α-glycosidic bonds (around 840 to 850 cm^{-1}) and β-glycosidic bonds (around 900

cm^{-1}). Moreover, the weak stretch band at 862 cm^{-1} and 763 cm^{-1} can be ascribed to α-pyranoses (α-D-glucose) in the EPS-LM (Asker et al., 2014; Saravanan and Shetty, 2016).

Furthermore, the presence of a peak at 1015 cm^{-1} is characteristic of the great chain flexibility of dextran around the α-(1→6) glycosidic bonds (Purama et al., 2009; Siddiqui et al., 2014; Yang et al., 2018). Taken together, analysis of FTIR spectra and constitutive monosaccharides of EPS-LM by HPTLC analysis, strongly support the hypothesis that EPS-LM is built-up of α-(1,6)-linked D-glucopyranosyl units. EPS-LM seems thus highly similar to dextran of *Leuconostoc mesenteroides* TDS2-19 (Du et al., 2017) NRRL B-640 (Purama et al., 2009), and FT045B (Vettori et al., 2012) strains.

Figure 3.

3.1.3. Zeta potential of EPS-LM and LTB toxin net charge and its physico-chemical analysis

Zeta potential values of EPS-LM were measured in sodium phosphate solutions adjusted to pH values ranging from 2 to 7 (Figure 4A). Zeta potential is the potential difference between the dispersion medium and the stationary layer of fluid attached to the dispersed particle (EPS-LM here). Zeta potential of EPS-LM was close to 0 mV at pH 2 and slightly decreased when pH increased reaching a ~ -10 mV value at pH 6. Nevertheless, the magnitude of this zeta potential value is far lower than that of "classical" charged polysaccharides, which have good stability in suspensions due to electrostatic repulsion (magnitude of zeta potential exceeding 40 mV). This observation is consistent with the fact that EPS-LM is composed likely dextran, which is a neutral polysaccharide, unlike anionic polysaccharides, such as alginates and pectins. In order to check whether electrostatic interactions between EPS-LM and LTB toxin are plausible, the net charge of LTB toxin as a function of pH was calculated with PepCalc.com-Peptide property calculator web server (Figure 4B). LTB toxin primary sequences have 103 amino acid residues. It can be observed that isoelectric pH value of LTB toxin is equal to 8.75. Consistently, LTB toxin has a net positive charge for a pH=7 value: this can be ascribed to the presence of positively charged amine groups such as lysine (Lys), arginine (Arg) and histidine (His) (basic side chains) at pH=7. Since EPS-LM had a slightly negative zeta potential value for a pH =7 value, electrostatic interaction with positively

charged LTB toxin cannot be excluded. Nevertheless, the contribution of other electrostatic interactions, such as hydrogen bonds or of hydrophobic interactions between EPS-LM and LTB toxin is likely to occur. Indeed, several biochemical processes, such as protein folding, their stability, and also their binding, are dominated by both hydrophobic and hydrophilic effects (Di Rienzo et al., 2021). In order to estimate the presence of hydrophobic and hydrophilic zones along the sequence of LTB toxin, hydropathy plot of LTB toxin is presented in Figure 5. This plot is consistent with LTB toxin structural analysis performed by van den Akker et al. (1996) who highlighted the positions that are part of the common hydrophobic core in the B subunits of the structures with a similar fold in the AB_5 toxin family.

Figure 4

Figure 5

3.2. SPR analysis

3.2.1. LTB toxin immobilization

In this work, the kinetic and thermodynamic parameters of the EPS binding to LTB toxin were estimated by using SPR analysis. A schematic illustration of LTB toxin immobilization on the gold sensor surface.is presented in Figure 6A. MUA is one of the ω-substituted alkane thiolates containing terminal functions, which consist of hydrophobic hydrocarbon chains and hydrophilic head groups. MUA molecules were chemisorbed on gold-coated surfaces via S-Au bonds to form combined self-assembled monolayers (SAMs). Then, the carboxyl groups of MUA were activated by EDC/NHS for the amine coupling of the LTB toxin (Dehghani et al., 2021). EDC/NHS coupling chemistry has been widely used for the development of systems such as biosensors, biochips, and lab-on-a-chip using biological molecules as the receptors. This method allows the free amine groups of the protein to covalently bind to the carboxyl groups created on the desired chip. Therefore, proteins can be stable during experiments by loading the ligand in the device (Kamra et al., 2016). To ensure the highest electrostatic interaction between the positively charged LTB toxin and negatively charged COO^--terminated MUA, the pH of the immobilization solution (sodium phosphate buffer, 10 mM) was 5.5 (Dehghani et al., 2021; Heggelund et al., 2019). As well, to block unreacted NHS sites with LTB toxin following its

immobilization, ethanolamine was applied to the chip. Steps of the recorded SPR sensorgram for immobilization of LTB toxin and its shift in angular resonance are depicted in Figure 1. After immobilization of LTB toxin, the initial resonance curve shifted to higher angles as the thickness of the adsorbed layer increased by about 0.32 deg. (i. e. from 69.26 to 69.58 deg.). This resulted from formation of a new layer on the gold chip.

Figure 6

3.2.2 Kinetics of LTB toxin interaction with EPS-LM

The SPR sensorgrams of EPS-LM/LTB toxin complex at three temperatures (298, 303, and 310 K) exhibited an increase in RU values when EPS-LM concentration increased (Figure. 7). Table 1 indicates values of kinetic parameters at three temperatures. According to these values, the kinetic constants (k_a and k_d) of the LTB toxin/EPS-LM complex increased regularly with temperature. Corresponding K_A values calculated at the three aforementioned temperatures were $(5.61 \pm 0.17) \times 10^5$ mol.L^{-1}, $(1.08 \pm 0.02) \times 10^6$ mol.L^{-1}, and $(2.05 \pm 0.04) \times 10^6$ mol.L^{-1}, respectively. These values indicate the high affinity of EPS-LM towards LTB toxin in the temperature range investigated (i. e. between 25°C and 37°C). Moreover, the values of K_A between LTB toxin and EPS-LM increased with temperature, which is demonstrative of an increase in EPS-LM binding to immobilized LTB toxin. This increase in affinity can be attributed to the observed increase of the association rate constants (k_a) when temperature increased. Indeed, calculated k_a values increased from 1.01×10^3 mol^{-1}.L.s at 25°C to 4.1×10^3 mol^{-1}.L.s at 37°C, while k_d values variations were lower.

It is likely that the enhanced binding of EPS-LM to LTB toxin at higher temperatures is related to the improvement of colliding EPS-LM molecules to the immobilized LTB toxin molecules on the chip surface and better diffusion of EPS-LM molecules. Extent of hydrogen bonding and electrostatic interactions between polysaccharide and protein can be related to the solution parameters such as pH, ionic strength, temperature etc. Besides electrostatic interactions, the presence of a few non-polar segments on both biopolymers can also result in hydrophobic interactions (Goh et al., 2020; Ghosh and Bandyopadhyay, 2012).

3.2.3. Thermodynamic analyses

To investigate the effect of temperature on thermodynamic characteristics, the interactions between EPS-LM and LTB toxin were investigated at different temperatures. According to the Van't Hoff equation, ΔH was calculated along with ΔS and ΔG through plotting ln K_A as a function of 1/T (Figure. 8). The intermolecular interactions between EPS-LM and immobilized LTB toxin might include hydrogen bonding, electrostatic, Van der Waals, and hydrophobic interactions. Their respective contributions can be assessed by calculating thermodynamic parameters of biomolecular interactions: the positive values of ΔH and ΔS (ΔH > 0 and ΔS > 0) imply hydrophobic forces, while when the values of both ΔH and ΔS are negative (ΔH < 0 and ΔS < 0), the main driving forces can be Van der Waals interactions and hydrogen bonds. Finally, if ΔH < 0 and ΔS > 0, this suggests that electrostatic interactions are dominating (Fathi et al., 2019).

The calculated thermodynamic parameters of EPS-LM - LTB toxin interaction are stated in Table 1. The positive values of ΔH and ΔS values suggest thus that the EPS-LM binds to LTB toxin mostly via hydrophobic interactions. Taking into account the structure of EPS-LM (OH-groups) and also the structure of LTB toxin protein, the calculated parameters resulting from thermodynamic analysis of SPR experiments seem to be rational. The ΔG values were negative revealing an exothermic binding phenomenon at all studied temperatures. As well, the increase of ΔG values with increasing the temperature demonstrates that the LTB toxin/EPS tends to decompose at higher temperatures (Afkham et al., 2022).

In general, electrostatic interactions are the main driving force for the complexation between proteins and charged polysaccharides (e. g. anionic ones such as alginate, or cationic ones such as chitosan). However, in the present case, EPS-LM have only a limited negative charge. Nevertheless, even when studying interactions between charged polysaccharides and proteins, several authors have reported that hydrogen bonding and hydrophobic interactions play an important secondary role in the stability of intermolecular attractions of their aggregates (McClements, 2006; Gentile, 2020). Moreover, the extent of hydrogen bonding and hydrophobic interaction also depends on temperature (Ghosh and Bandyopadhyay, 2012). Previous researchers have also characterized binding interactions between α-glucans from *Lactobacillus reuteri* and milk proteins (such as β-lactoglobulin and κ-casein) by surface

plasmon resonance. In fact, glucans with multiple α-(1,6) linkages had the highest binding levels to κ-casein, whereas α-(1,6) linkages reduced the interaction with native β-lactoglobulin. In general, glycosidic linkage types, branching and molecular weight of the EPS can affect interactions with milk protein (Diemer et al., 2012).

Figure 7

Figure 8

Table 1

3.3. Docking Studies

To predict the best conformation of the LTB toxin/EPS-LM complexes and the most favorable binding pose and binding energy prediction in the whole protein molecule, the researchers have proposed blind protein-ligand docking methods in addition to using the domain-based docking procedure. In the first procedure, the lowest predicted binding energy or E_{lowest} ($kJ.mol^{-1}$), which refers to ΔG ($kJ.mol^{-1}$), regarding the output of AutoDock vina, results (with the performance of 6 mode runs) in the whole EPS-LM structure was considered meticulously to achieve the best conformation of LTB toxin/EPS-LM complex. However, the most stable LTB toxin/EPS-LM complex belonged to the conformation with lower predicted binding energy with $\Delta G = -7.8$ kJ. mol^{-1}.

To complement practical studies, the EPS-LM was docked to LTB toxin to determine the possible binding sites. Docking studies are shown in Figure 9. According to our results, the EPS-LM was bound to LTB toxin with a hydrophobic core, but it apparently interacted with EPS-LM in a deep recess on the LTB toxin surface. The amino acids involved in hydrophobic bonds include Glu66, Lys63, Asp70, and Arg67. This zone of LTB toxin seems to involve binding with the biological targets responsible for its toxin activity that are able to interact with it hydrophobically. In designed ligand, the EPS OH-groups play an important role in connecting to the LTB toxin. Therefore, in Autodock Vina software, LTB toxin was able to form a hydrogen bond with the Glu66 amino acid. However, after studies with LigPlot software, in addition to the mentioned bonds, EPS-LM is surrounded by Glu66, Arg67, Asp70, and

Lys63. In general, the results predicted using the above method were consistent with the results obtained with the SPR method.

Figure 9

The hydrophobic and hydrophilic regions in the secondary structure of involved α-helix domain peptides in inner regions of LTB toxin were predicted using Schiffer-Edmundson helical wheel modeling (Figure. 10). LTB toxin α-helix was predicted to form an amphipathic α-helix, with the full sequence: SQKKAIERMKDTLRITYLTE. Polar and non-polar residues of α-helix region were readily estimated in Figure 10. According to our results, physico-chemical properties of LTB toxin were used to estimate hydrophobicity <H> and hydrophobic moment <μH> with 0.149 and 0.227 values, respectively. In fact, sequence length and analysis window were selected: 20 amino acids showing a clear hydrophobic slant on one side (hydrophobic face: Leu, Ile, Tyr), while on the other side hydrophilic residues were present. In other words, EPS-LM can also closely approach the hydrophobic surface formed by hydrophobic face containing the side chains of residue Leu, Ile, Tyr. However, this region seems likely to have a more limited amphipathicity, since some hydrophilic residues (13 amino acids / 65 %) might interfere with the hydrophobic side (7 amino acids/35 %). Therefore, B subunits of these heterohexameric AB_5 toxins form a pentameric arrangement, which is possible for binding to each other with similar folds through these residues, nevertheless charged residues such as Arg3, Lys2, Glu2 and Asp1 can be important, as well. In general, the hydrophobic core of LTB toxin can be able to form favorable non-polar and polar interactions with the protein's binding surface with carbohydrate derivations such as galactose, particularly with amino acids residues such as Lys, Arg, Asn, Ile, Gly, Glu (Fan et al., 2001). However, as mentioned above, this is most likely an indication that non-specific hydrophobic interactions with the α-helix region increase EPS-LM binding affinity more than hydrophilic bindings.

Figure 10

4. Conclusion

In this study, the interactions between EPS-LM and LTB toxin from *Escherichia coli* were investigated using the SPR technique, following LTB toxin immobilization on chips, and molecular docking analysis. Kinetic study showed that the affinity of EPS-LM to LTB toxin was high, which was confirmed by the high value of K_A. Thermodynamic investigations suggested that the dominant forces between EPS-LM and LTB toxin were hydrophobic interactions owing to the hydrophobic characteristic of LTB toxin, and these results were confirmed with molecular docking studies, also indicating the contribution of a hydrogen bond in their complexation. K_A of LTB toxin interaction with EPS-LM increased upon rising temperature, which indicated that affinity between these biomolecules increase upon rising temperatures. As well, the negative value of ΔG demonstrated that the binding of these two biomolecules is entropy-driven and spontaneous. The docking studies and Schiffer–Edmundson helical wheel diagrams of LTB toxin indicated the hydrophobic core that seems a highly effective region interacting with EPS-LM. Considering the high affinity of *Leuconostoc mesenteroides* P35 exopolysaccharides for *Escherichia coli* heat-labile enterotoxin at physiological temperatures and pH, these polysaccharides have a good potential to complex this toxin and thereby limit its toxicity. Further studies are thus needed to check whether *Leuconostoc mesenteroides* P35 exopolysaccharides could effectively limit the toxicity of *Escherichia coli* heat-labile enterotoxin.

Acknowledgments

The authors thank the Ministère des Affaires Etrangères (France) and the Ministry of Research, Science and Technology (Iran) for financing double PhD scholarship joint-supervision program between France and Iran for Mojtaba AZARI-ANPAR. The authors are indebted to Conseil Départemental de l'Ain and Bourg en Bresse Agglomération for the financial support of BioDyMIA research unit activities.

References

Afkham, S., Hanaee, J., Zakariazadeh, M., Fathi, F., Shafiee, S., & Soltani S. (2022). Molecular mechanism and thermodynamic study of rosuvastatin interaction with human serum albumin using a

surface plasmon resonance method combined with a multi-spectroscopic, and molecular modeling approach. *European Journal of Pharmaceutical Sciences*, *168*, 106005.

Asker, M.M.S., Sayed, O.H.E., Mahmoud, M.G., & Ramadan, M.F. (2014). Chemical structure and antioxidant activity of a new exopolysaccharide produced from *Micrococcus luteus*. *Journal of Genetic Engineering and Biotechnology*, *12*, 121-126.

Ayala-Torres, C., Hernández, N., Galeano, A., Novoa-Aponte, L., & Soto, C.Y. (2014). Zeta potential as a measure of the surface charge of mycobacterial cells. *Annals of Microbiology*, *64*, 1189-1195.

Benvidi, S.M.H., & Jahanbin, K. (2020). A new water-soluble polysaccharide from *Echinops pungens* Trautv roots. Part I. Isolation, purification, characterization and antioxidant activity. *International Journal of Biological Macromolecules*, *161*, 909-916.

Chen, J.-C., Ho, T.-Y., Chang, Y.-S., Wu, S.-L., & Hsiang, C.-Y. (2006). Anti-diarrheal effect of *Galla Chinensis* on the *Escherichia coli* heat-labile enterotoxin and ganglioside interaction. *Journal of Ethnopharmacology*, *103*, 385-391.

Chen, J.-C., Ho, T.-Y., Chang, Y.-S., Wu, S.-L., Li, C.-C., & Hsiang, C.-Y. (2009). Identification of *Escherichia coli* enterotoxin inhibitors from traditional medicinal herbs by *in silico*, *in vitro*, and *in vivo* analyses. *Journal of Ethnopharmacology*, *121*, 372-378.

Dehghani, M., Jalal, R., & Rashidi, M.R. (2021). Kinetic and thermodynamic insights into the interaction of Aβ1-42 with astaxanthin and aggregation behavior of Aβ1-42: Surface plasmon resonance, microscopic, and molecular docking studies. *Biophysical Chemistry*, *275*, 106612.

Di Rienzo, L., Miotto, M., Bò L., Ruocco, G., Raimondo, & D., Milanetti, E. (2021). Characterizing hydropathy of amino acid side chain in a protein environment by investigating the structural changes of water molecules network. *Frontiers in Molecular Biosciences*, *8*, 626837.

Diemer, S.K., Svensson, B., Babol, L.N., Cockburn, D., Grijpstra, P., Dijkhuizen, L., Folkenberg, D.M., Garrigues, C., & Ipsen, R.H. (2012). Binding interactions between α-glucans from *Lactobacillus reuteri* and milk proteins characterised by surface plasmon resonance. *Food Biophysics*, *7*, 220-226.

Diemer, S.K., Svensson, B., Babol, L.N., Cockburn, D., Grijpstra, P., Dijkhuizen, L., Folkenberg, D.M., Garrigues, C. & Ipsen, R.H. (2012). Binding Interactions Between α-glucans from Lactobacillus reuteri and Milk Proteins Characterised by Surface Plasmon Resonance. *Food Biophysics*, *7*(3), pp.220-226.

Du, R., Xing, H., Yang, Y., Jiang, H., Zhou, Z., & Han, Y. (2017). Optimization, purification and structural characterization of a dextran produced by *L. mesenteroides* isolated from Chinese sauerkraut. *Carbohydrate Polymers*, *174*, 409-416.

Fan, E., Merritt, E.A., Zhang, Z., Pickens, J.C., Roach, C., Ahn, M., & Hol, W.G. (2001). Exploration of the GM1 receptor-binding site of heat-labile enterotoxin and cholera toxin by phenyl-ring-containing galactose derivatives. *Acta Crystallographica Section D: Biological Crystallography*, *57*, 201-212.

Fathi, F., Sharifi, M., Jafari, A., Kakavandi, N., Kashanian, S., Dolatabadi, J.E.N., & Rashidi, M.R. (2019). Kinetic and thermodynamic insights into interaction of albumin with piperacillin: spectroscopic and molecular modeling approaches. *Journal of Molecular Liquids*, *296*, 111770.

Gemelas, L., Degraeve, P., Hallier, A., & Demarigny, Y. (2018). Development of a fermented dairy product as an ingredient to be added to low-fat bakery goods: Instrumental and sensory analyses of textural and aromatic characteristics. *Journal of Pure and Applied Microbiology*, *12*, 1061-1069.

Gentile, L. (2020). Protein-polysaccharide interactions and aggregates in food formulations. *Current Opinion in Colloid and Interface Science*, *48*, 18-27.

Ghosh, A.K., & Bandyopadhyay, P. (2012). Polysaccharide-protein interactions and their relevance in food colloids. *The Complex World of Polysaccharides*, *14*, 395-406.

Goh, K.K., Teo, A., Sarkar, A., & Singh, H. (2020). Milk protein-polysaccharide interactions. In *Milk proteins* (pp. 499-535). Academic Press.

Heggelund, J.E., Heim, J.B., Bajc, G., Hodnik, V., Anderluh, G., & Krengel, U. (2019). Specificity of *Escherichia coli* heat-labile enterotoxin investigated by single-site mutagenesis and crystallography. *International Journal of Molecular Sciences*, *20*, 703.

Hiemenz, P.C., & Rajagopalan, R. (1977). Electrophoresis and other electrokinetic phenomena. In: Lagowski, J.J., Principles of Colloid and Surface Chemistry, *3*, pp.544-550.

Jiménez-Vargas, J.M., Ramírez-Carreto, S., Corzo, G., Possani, L.D., Becerril, B., & Ortiz, E. (2021). Structural and functional characterization of NDBP-4 family antimicrobial peptides from the scorpion *Mesomexovis variegatus*. *Peptides*, *141*, 170553.

Jurášková, D., Ribeiro, S.C., & Silva, C.C.G. (2022). Exopolysaccharides produced by lactic acid bacteria: from biosynthesis to health-promoting properties. *Foods*, *11*, 156.

Kamra, T., Chaudhary, S., Xu, C., Montelius, L., Schnadt, J., & Ye, L. (2016). Covalent immobilization of molecularly imprinted polymer nanoparticles on a gold surface using carbodiimide coupling for chemical sensing. *Journal of Colloid and Interface Science*, *461*, 1-8.

McClements, D.J. (2006) Non-covalent interactions between proteins and polysaccharides, *Biotechnology advances*, *24(6)*, (2006) 621-625.

Nambiar, R.B., Sellamuthu, P.S., Perumal, A.B., Sadiku, E.R., Phiri, G., & Jayaramudu, J. (2018). Characterization of an exopolysaccharide produced by *Lactobacillus plantarum* HM47 isolated from human breast milk. *Process Biochemistry*, *73*, 15-22.

Oshannessy, D.J., Brighamburke, M., Soneson, K.K., Hensley, P. & Brooks, I., (1993). Determination of rate and equilibrium binding constants for macromolecular interactions using surface plasmon resonance: use of nonlinear least squares analysis methods. *Analytical biochemistry*, *212*(2), pp.457-468.

Pickens, J.C., Merritt, E.A., Ahn, M., Verlinde, C.L., Hol, W.G., & Fan, E. (2002). Anchor-based design of improved cholera toxin and *E. coli* heat labile enterotoxin receptor binding antagonists that display multiple binding modes. *Chemistry and Biology*, *9*, 215-224.

Purama, R.K., Goswami, P., Khan, A.T., & Goyal, A. (2009). Structural analysis and properties of dextran produced by *Leuconostoc mesenteroides* NRRL B-640. *Carbohydrate Polymers*, *76*, 30-35.

Saravanan, C., & Shetty, P.K.H. (2016). Isolation and characterization of exopolysaccharide from *Leuconostoc lactis* KC117496 isolated from idli batter. *International Journal of Biological Macromolecules*, *90*, 100-106.

Shingel, K.I. (2002). Determination of structural peculiarities of dexran, pullulan and γ-irradiated pullulan by Fourier-transform IR spectroscopy. *Carbohydrate Research*, *337*, 1445-1451.

Siddiqui, N.N., Aman, A., Silipo, A., Qader, S.A.U., & Molinaro, A. (2014). Structural analysis and characterization of dextran produced by wild and mutant strains of *Leuconostoc mesenteroides*. *Carbohydrate Polymers*, *99*, 331-338.

Srednicka, P., Juszczuk-Kubiak, E., Wojcicki, M., Akimowicz, M., & Roszko, M.L. (2021). Probiotics as a biological detoxification tool of food chemical contamination: A review. *Food and Chemical Toxicology*, *153*, 112306.

van den Akker, F., Sarfaty, S., Twiddy, E.M., Connell, T.D., Holmes, R.K., Hol, W.G. (1996). Crystal structure of a new heat-labile enterotoxin, LT-IIb. *Structure*, *4*, 665-678.

Vettori, M.H.P.B., Franchetti, S.M.M., & Contiero, J. (2012). Structural characterization of a new dextran with a low degree of branching produced by *Leuconostoc mesenteroides* FT045B dextransucrase. *Carbohydrate Polymers*, *88*, 1440-1444.

Yang, Y., Feng, F., Zhou, Q., Zhao, F., Du, R., Zhou, Z., & Han, Y. (2018). Isolation, purification and characterization of exopolysaccharide produced by *Leuconostoc pseudomesenteroides* YF32 from soybean paste. *International Journal of Biological Macromolecules*, *114*, 529-535.

Zhang, Z., Cai, R., Zhang, W., Fu, Y., & Jiao, N. (2017). A novel exopolysaccharide with metal adsorption capacity produced by a marine bacterium *Alteromonas* sp. JL2810. *Marine Drugs*, *15*, 175.

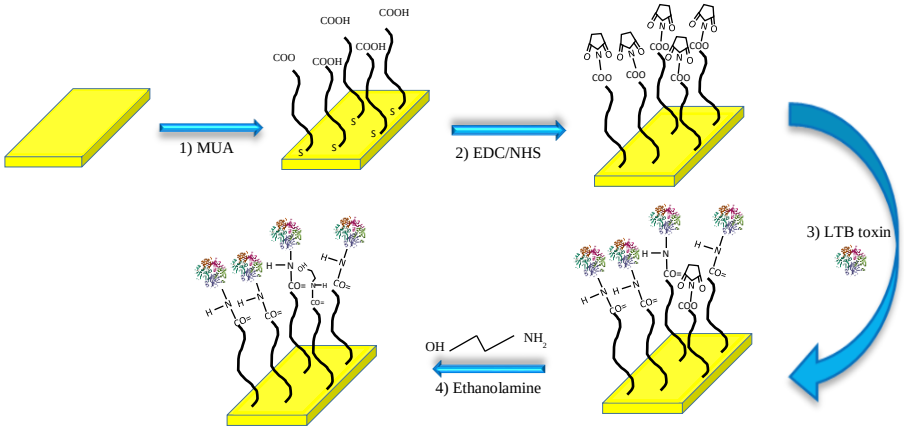

Fig 1. Schematic illustration of *Escherichia coli* heat-labile enterotoxin B-pentamer (LTB toxin) immobilization by amine coupling: (1) carboxymethyl dextran sensor chip (2) Activation of COOH groups in CMD by EDC/NHS (3) Immobilization of the LTB toxin (4) Deactivation of the remaining activated surface groups through capping by ethanolamine.

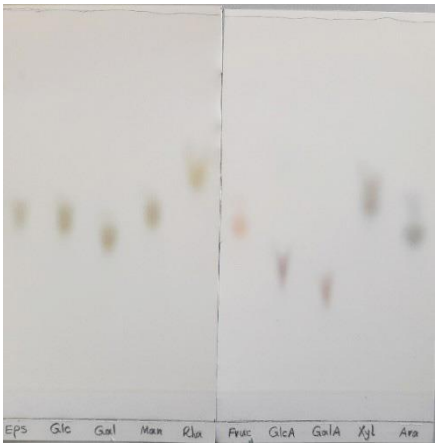

Figure 2. HPTLC plate with hydrolyzed samples of EPS-LM and standard monosaccharides.

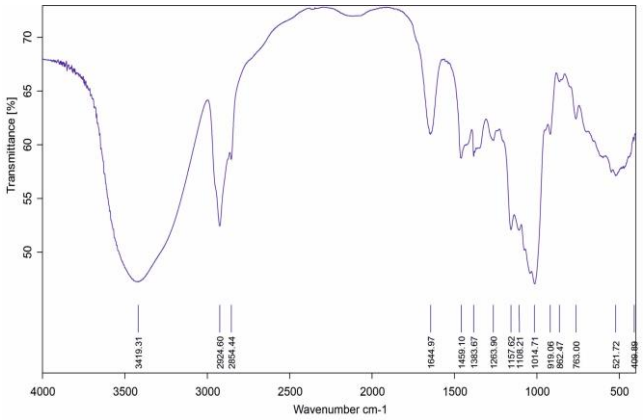

Figure 3. FT-IR spectrum of EPS-LM

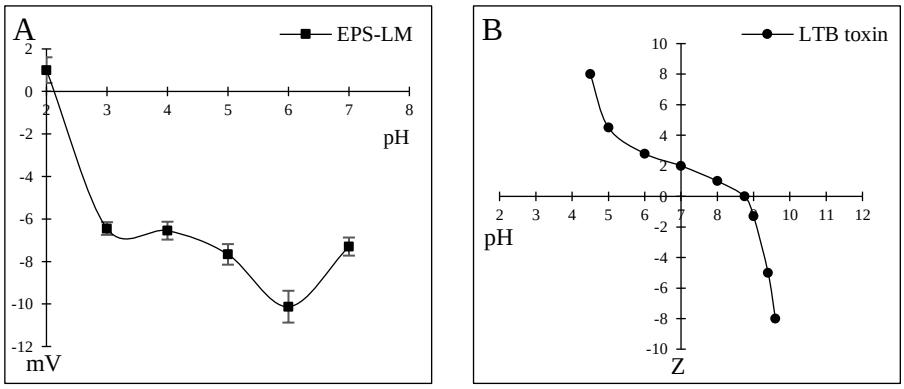

Figure 4: A. Zeta potential of EPS-LM as a function of pH (2–7) in 10 mM sodium phosphate buffer at 23 °C. B. estimation of net charge of LTB toxin as a function of pH by using PepCalc.com-Peptide property calculator web server.

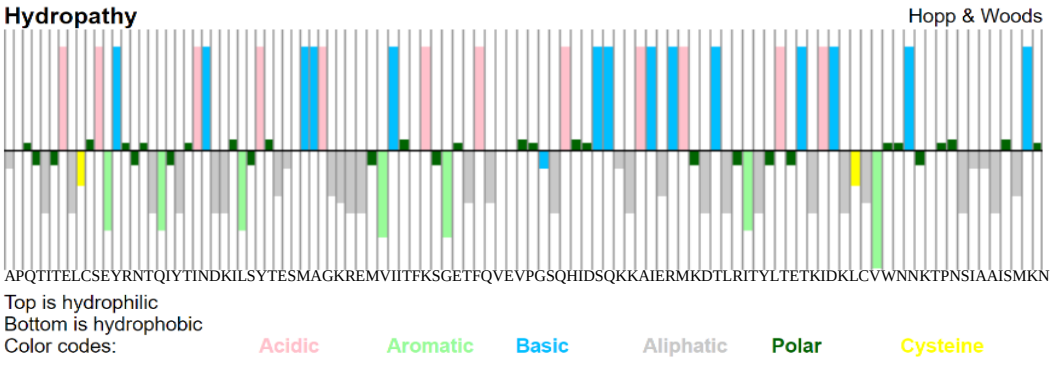

Figure 5: Hydropathy plot of LTB toxin.

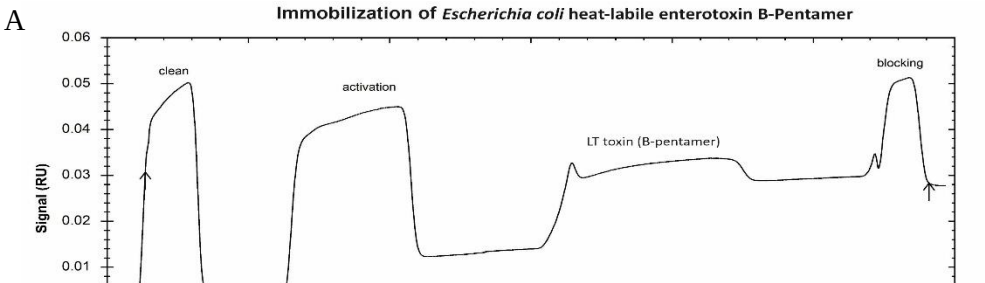

B

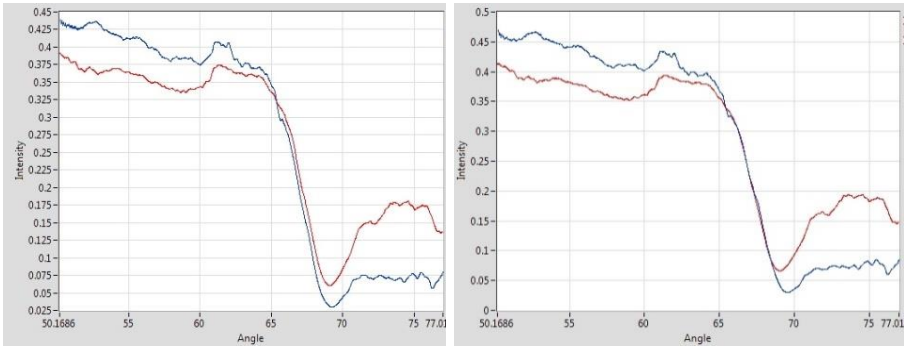

Figure 6. A) SPR sensorgram of LTB toxin immobilization processes on a carboxymethyl dextran (CMD) hydrogel sensor chip; **B**) Initial SPR curve before (left) and after (right) LTB toxin immobilization.

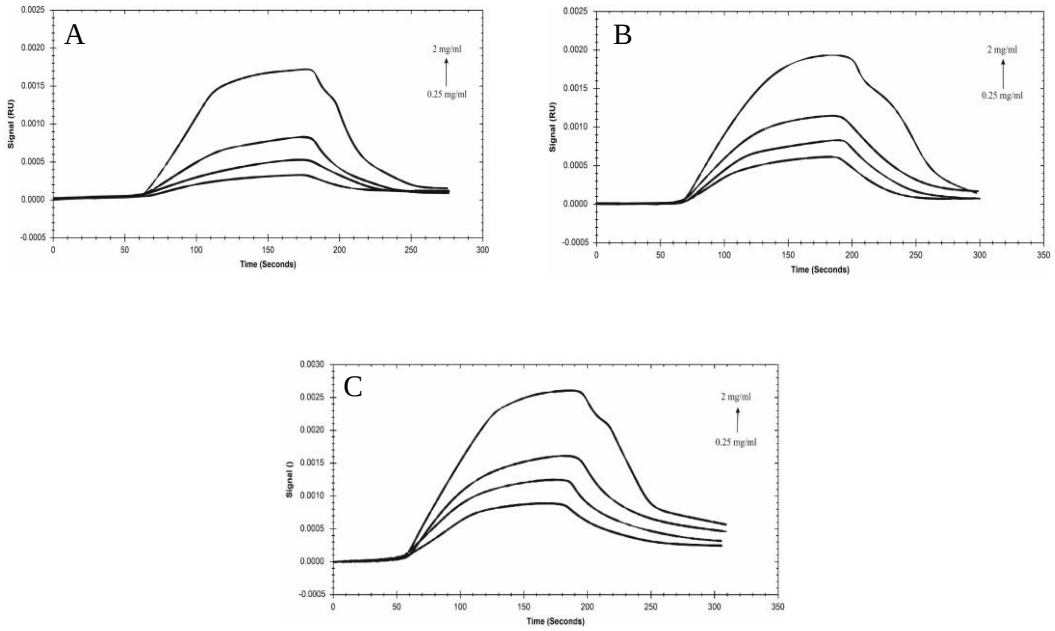

Fig 7. SPR sensorgrams of interaction of EPS-LM at different concentrations (0.25-2 $g.L^{-1}$ in sodium phosphate buffer (10 mM, pH 7) with LTB toxin immobilized on a carboxymethyl dextran (CMD) hydrogel sensor chip at 298 K (A), 303 K (B) ,and 310 K (C).

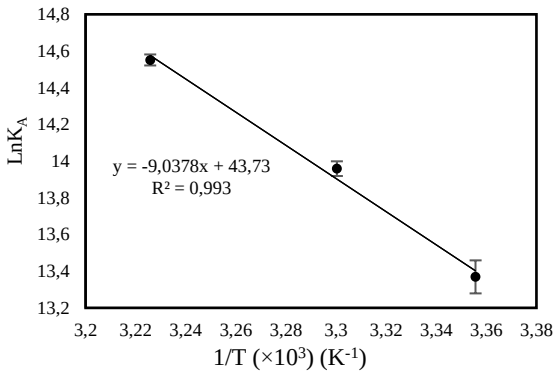

Figure 8. Van't Hoff plot for the interaction of EPS-LM with immobilized LTB toxin.

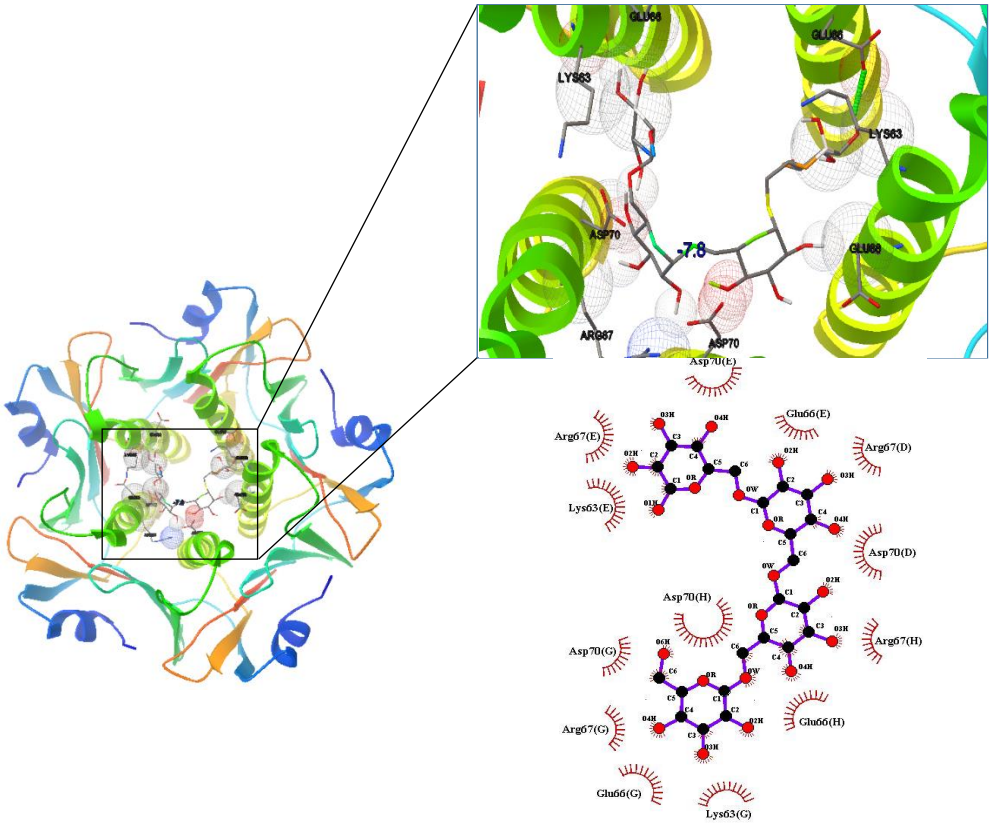

Figure 9. Molecular docking studies of putative interactions between LTB toxin and EPS-LM.

$_{1}$SQKKAIERMKDTLRITYLTE$_{20}$		
Physico-chemical properties	**Polar residues + GLY**	**Nonpolar residues**
Hydrophobicity <H>	**Polar residues + GLY (n / %)**	**Nonpolar residues (n / %)**
0.149	13 / 65.00	7 / 35.00
Hydrophobic moment <μH>	**Uncharged residues + GLY**	**Aromatic residues**
0.227	GLN 1, SER 1, THR 3, GLY 0	TYR 1,
Net charge z	**Charged residues**	**Special residues**
2	LYS 3, ARG 2, GLU 2, ASP 1,	CYS 0, PRO 0
Hydrophobic face : L I Y		

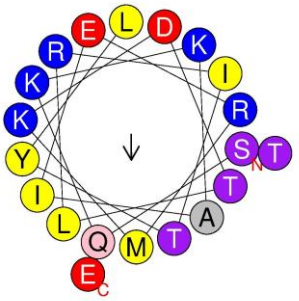

Figure 10. Schiffer-Edmundson helical wheel diagrams of LTB toxin in its α-helix domain by using the HeliQuest web server. Positively charged residues are shown in blue circles, negatively charged residues in red, hydrophobic residues in yellow, hydrophilic residues in purple, amide residues in pink, and small residues in grey. The direction of the hydrophobic moments is shown by arrows. The red N and C represent the peptide sequence's N- and C-termini, respectively. H stands for peptide

Table 1. Association rate constant (k_a), dissociation rate constant (k_d), and equilibrium constants (K_A) values of LTB toxin interaction with EPS-LM.

Temperature (K)	**k_a ($mol^{-1}.L.s$)**	**k_d (s^{-1})**	**K_A ($mol.L^{-1}$)**	**ΔH ($kJ.mol^{-1}$)**	**ΔS ($J.mol^{-1}$)**	**ΔG ($kJ.mol^{-1}.K^{-1}$)**
298	$(1.21 \pm 0.2) \times 10^{3}$	$(1.88 \pm 0.02) \times 10^{-3}$	$(5.61 \pm 0.17) \times 10^{5}$			-32.79± 0.37
303	$(1.58 \pm 0.2) \times 10^{3}$	$(1.37 \pm 0.1) \times 10^{-3}$	$(1.08 \pm 0.02) \times 10^{6}$	0.082± 0.01	386.02± 2.6	-35.01± 0.10
310	$(4.60 \pm 0.5) \times 10^{3}$	$(2.2 \pm 0.2) \times 10^{-3}$	$(2.05 \pm 0.04) \times 10^{6}$			-37.46± 0.05